



## A novel strategy for tailoring Ag-ZnO nanowires for photocatalytic mercury removal

Khadijah S. Al-Namshah

College of Science, Main Campus King Abdullah Rd, King Khalid University, Abha, Saudi Arabia, email: Drknamshah@gmail.com

Received 19 January 2018; Accepted 8 July 2018

### ABSTRACT

Ag-ZnO nanocomposites were synthesized in an effective manner to produce uniformly structured nanowires. These nanocomposites were then used for mercury(II) reduction. Synthesis conditions, heat treatment, and other factors that affect the structure properties of the nanocomposite were extensively studied to optimize the synthesis conditions. Ag-ZnO nanocomposites were prepared by a sol-gel route. The specific surface area values for ZnO (Z), 0.4 wt % Ag-ZnO (AGZ-0.4), 0.8 wt % Ag-ZnO (AGZ-0.8), 1.2 wt % Ag-ZnO (AGZ-1.2) and 1.6 wt % Ag-ZnO (AGZ-1.6) nanocomposites were determined to be 60, 56, 53, 50 and 48 m<sup>2</sup>/g, respectively. The reduction of mercury(II) under visible light was used to study the photocatalytic performance of the nanocomposites. In terms of photocatalytic performance for mercury(II) reduction, AGZ-1.2 outperforms AGZ-1.6 by 0.99 times, AGZ-0.8 by 1.2 times, AGZ-0.4 by 1.98 times, and Z by 24.75 times.

*Keywords:* ZnO; Silver; Nanowires; Mercury(II); Visible light

### 1. Introduction

Many industries, such as the electronic, electrical industry and chlorine-alkali industry, use mercury. Mercury compounds are used as catalysts in petrochemical and chemical industries for many processes, such as dehydrogenation, hydrogenation, chlorination, oxidation, sulfonation, and plastics production [1]. The toxicity of mercury compounds is very high. Mercury compounds affect the central nervous system in both humans and animals [2]. Mercury compounds cause pollution to human health. Many of the fisheries are contaminated by a high level of mercury due to inhalation of mercury vapor through fish consumption [3,4]. To protect the populations from mercury poisoning, most governments on Earth have suggested safe levels for fish consumption and also adopted seafood consumption advisories [5]. Additionally, the rate of natural degradation for mercury is very low. Therefore, the contamination by mercury must be removed. The most famous methods used for removal of mercury(II) are based on adsorption,

ion exchange, reduction and precipitation as sulfide [1,6,7]. Recently, a photocatalysis process has been used for removal of mercury using titanium dioxide as photocatalyst [8–12]. In this process, the removal of mercury was realized by conversion of divalent mercury species to elemental mercury via a reduction process using photogenerated electrons in titanium dioxide [10,12]. Additionally, no removal of mercury was found in the absence of titanium dioxide and presence of ultraviolet (UV) light [10,12]. In the presence of methanol, formic and citric acid as an organic scavenger, the removal of mercury was increased due to the scavenger-induced prevention or reduction in e<sup>-</sup>-h<sup>+</sup> pair recombination [13]. Although, TiO<sub>2</sub> is a well-known photocatalyst, its commercialization is hindered by two problems: first, is its absorption in the UV region and second the agglomeration of nanoparticles [14]. Many methods have been used to overcome these two problems. One such method is to convert the absorption of titanium dioxide from the UV region to the visible region by doping of metals or nonmetals [15–28]. In this work, the agglomeration of zinc oxide was overcome by preparing zinc-oxide nanowires. The wide bandgap of zinc oxide was overcome by silver doping zinc oxide. Zinc oxide and Ag-ZnO nanowires were characterized using many

\* Corresponding author.

different characterization techniques and the photocatalyst performance was studied for the reduction of mercury species.

## 2. Experimental

### 2.1. Preparation of ZnO nanowires

0.3 mol of zinc methoxide is dissolved in deionized water (10 mL) and 30 mL of methanol followed by the addition of ethylene glycol and citric acid (molar ratio = 4:1) for forming the polymeric matrix. The citric acid to total metal ions molar ratio was kept constant at 1:1. Ammonium hydroxide solution was used to adjust the solution pH to 8.0. A transparent sol was obtained after continuous stirring of the above mixture for 2 h at 303 K. The gel was formed after aging a transparent sol at room temperature. ZnO nanowires were obtained after drying the gel for 24 h at 353 K followed by calcination for 3 h at 873 K.

### 2.2. Ag-ZnO nanowires

Ag-ZnO nanowires were prepared using a photoassisted deposition method. Different weight percents of silver nitrate were dissolved in deionized water (100 mL) to obtain different weight percent of silver such as 0.4, 0.8, 1.2, or 1.6 wt % Ag. Then, 1 g of ZnO was dispersed in an aqueous solution of silver nitrate. A UV lamp was used to irradiate the obtained mixture for 24 h. The Ag-ZnO nanowires were obtained after drying the obtained materials for 24 h at 353 K.

### 2.3. Characterization of the photocatalysts

A JEOL-JEM-1230 transmission electron microscope (TEM) was used to obtain the morphology and sample dimensions for the prepared materials. To obtain the TEM images, samples were ultrasonicated for 30 min after suspension in ethanol. A small portion of the suspended sample was dried on a carbon-coated copper grid and loaded into the spectrometer.

The structure morphology for ZnO and Ag/ZnO nanowires was measured using a scanning electron microscope (SEM) model: JEOL-JSM-5410.

The surface area was calculated from N<sub>2</sub>-adsorption measurements for the sample at 77 K using a Nova 2000 series Chromatech apparatus. Samples were heated at 453 K under vacuum for 2 h to complete this measurement.

A Bruker axis D8 X-ray diffraction (XRD) system was used to observe the crystalline phase of the nanocomposites. XRD was performed by utilizing Cu K $\alpha$  radiation ( $\lambda = 1.540 \text{ \AA}$ ) at room temperature.

A Thermo-Scientific K-ALPHA spectrometer was used to obtain X-ray photoelectron spectroscopy (XPS) measurements. A UV-Vis-NIR spectrophotometer (V-570, Jasco, Japan) was used to measure ultraviolet-visible diffuse reflectance spectra (UV-Vis-DRS); these spectra were observed at room temperature over an absorption range of 200–800 nm. The bandgap performance was determined from the observed UV-Vis-DRS. A Shimadzu RF-5301 fluorescence spectrophotometer was used to record the photoluminescence emission spectra (PL).

### 2.4. Photocatalytic tests

The efficiency of the prepared nanocomposites was tested for the reduction of mercury ions. For this purpose, a known weight of the photocatalyst was ultrasonically dispersed in 500 mL of mercury(II) chloride solution with an initial concentration of mercury(II) of 100 ppm. The reaction mixture was illuminated under artificial visible light produced from a 500 W Xenon lamp mounted on a photocatalytic reactor. A  $\lambda > 420 \text{ nm}$  cutoff filter was used and a running water tube was exploited to prevent heating, which enabled the reaction solution temperature to be kept constant at approximately 303 K. The sealed quartz reactor was placed 11 cm from the light source. Before illumination, dissolved oxygen was flushed from the solution by nitrogen for 0.5 h. The illumination time was set to 1 h for each experiment. After exposure, samples were drawn from the reactor, centrifuged at 7,000 rpm for 20 min and then finally filtered through a 0.2- $\mu\text{m}$  Millipore filter to remove any residual particles. A UV/Vis/NIR spectrophotometer model: V-570, JASCO, Japan was used to analyze the remaining mercury(II) following the reduction process.

## 3. Results and discussion

### 3.1. Characterization of materials

Fig. 1 shows XRD patterns for Z, AGZ-0.4, AGZ-0.8, AGZ-1.2, and AGZ-1.6 samples. The broad peaks at 31.8°, 34.5°, 36.3°, 47.6°, 56.7°, 62.9°, 67.0°, and 68.1° suggest a zinc oxide phase structure for Z and AGZ samples. No peaks for silver or silver oxide were observed for the AGZ samples due to a high dispersion of silver on the zinc oxide surface. Additionally, the decrease in intensity of the characteristic peaks of ZnO phase in the spectra for the AGZ samples suggests that the doping of silver decreases the crystallite sizes in the ZnO phase.

Fig. 2 shows SEM images for Z, AGZ-0.4, AGZ-0.8, AGZ-1.2, and AGZ-1.6 samples. Z, AGZ-0.4, AGZ-0.8, AGZ-1.2,

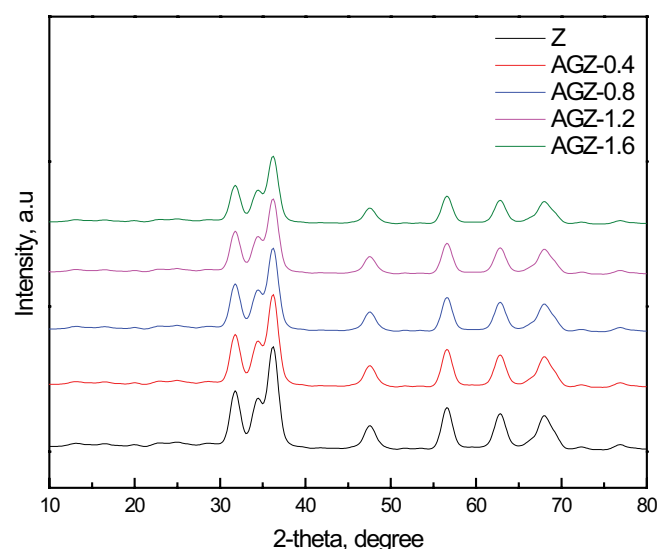


Fig. 1. XRD patterns for the Z, AGZ-0.4, AGZ-0.8, AGZ-1.2, and AGZ-1.6 samples.

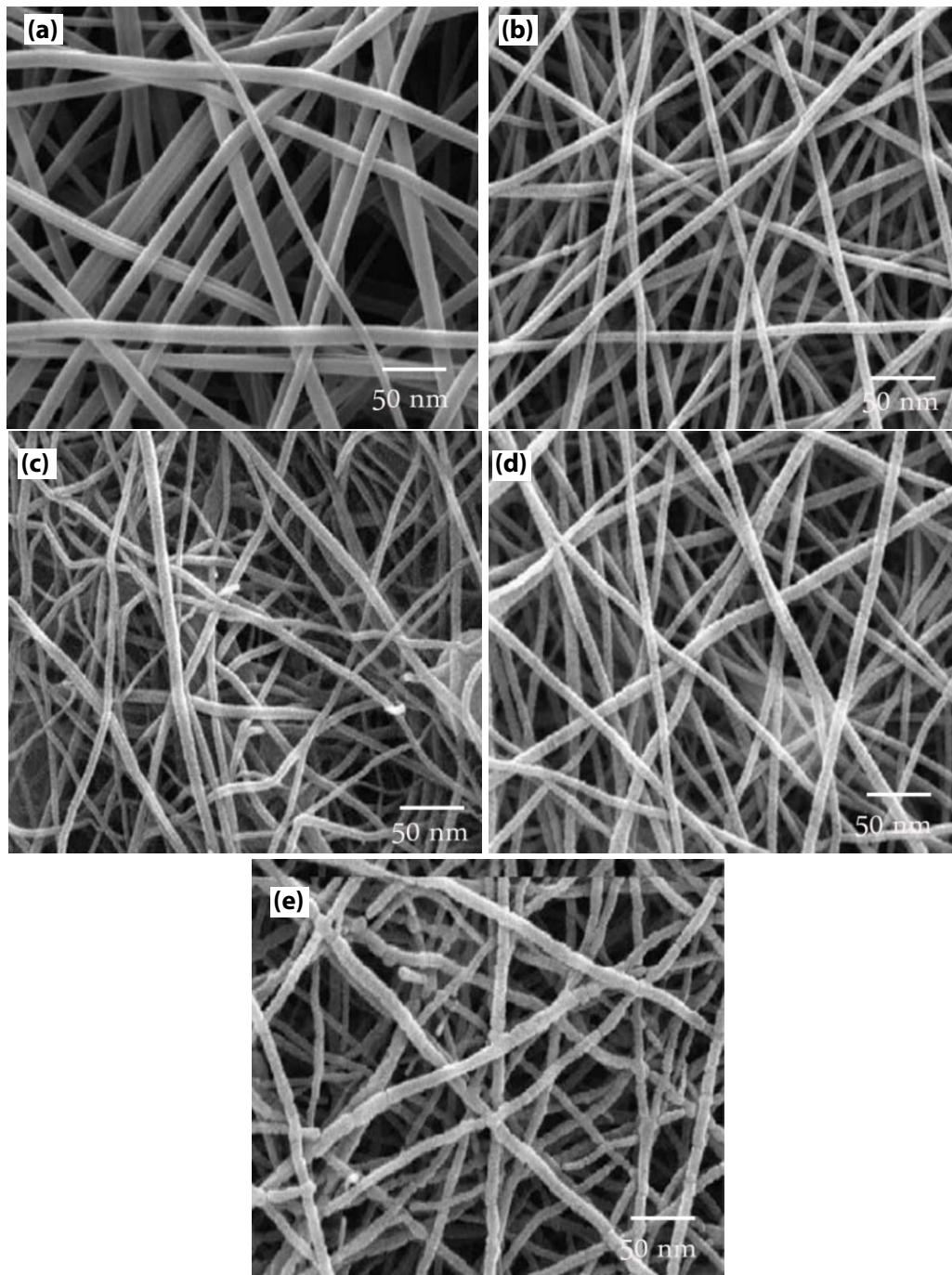


Fig. 2. SEM images for the Z (a), AGZ-0.4 (b), AGZ-0.8 (c), AGZ-1.2 (d), and AGZ-1.6 (e) samples.

and AGZ-1.6 samples show a nanowire shape. However, AGZ-0.4, AGZ-0.8, AGZ-1.2, and AGZ-1.6 samples are nanowires in shape and also covered by silver. It is clear that the addition of silver decreases the size of the ZnO nanowires.

Fig. 3 shows TEM images for the Z and AGZ-1.2 samples. The Z and AGZ-1.2 samples are nanowires in shape. The addition of silver to ZnO decreases the size of the ZnO sample and silver appears as a dot on the surface of the ZnO nanowires.

XPS spectra for Ag3d for the AGZ-1.2 sample are shown in Fig. 4. The presence of two binding peaks for Ag3d<sub>5/2</sub> and Ag3d<sub>3/2</sub> at 367.5 and 368.1 eV indicate that the silver is metallic silver [29].

The specific surface area for the Z, AGZ-0.4, AGZ-0.8, AGZ-1.2, and AGZ-1.6 samples was also measured. Z, AGZ-0.4, AGZ-0.8, AGZ-1.2, and AGZ-1.6 samples were measured by a Nova 2000 resulting in values of 60, 56, 53, 50, and 48 m<sup>2</sup>/g, respectively, as shown in Table 1. Therefore, the nanowire structure for the zinc oxide increases the BET

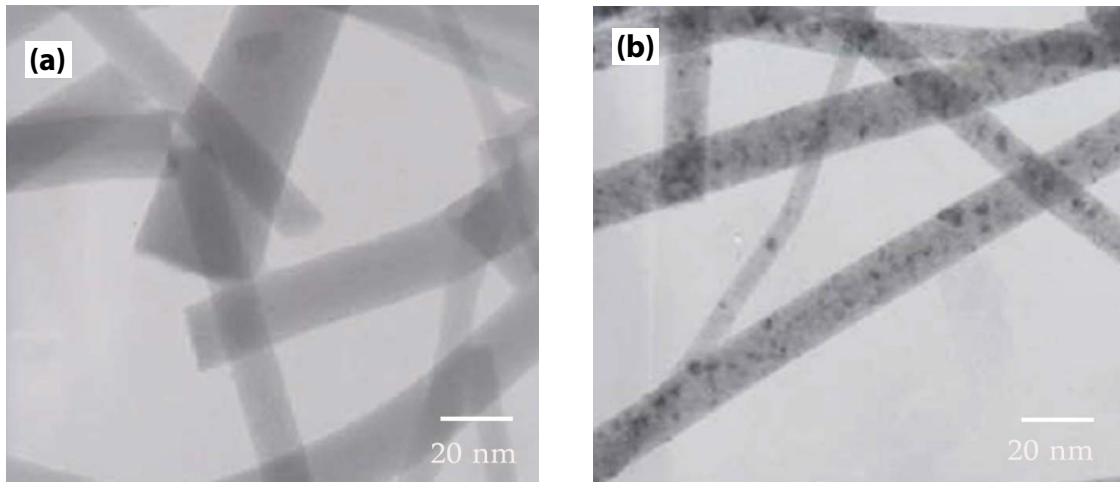


Fig. 3. TEM images for the Z (a) and AGZ-1.2 (b) samples.

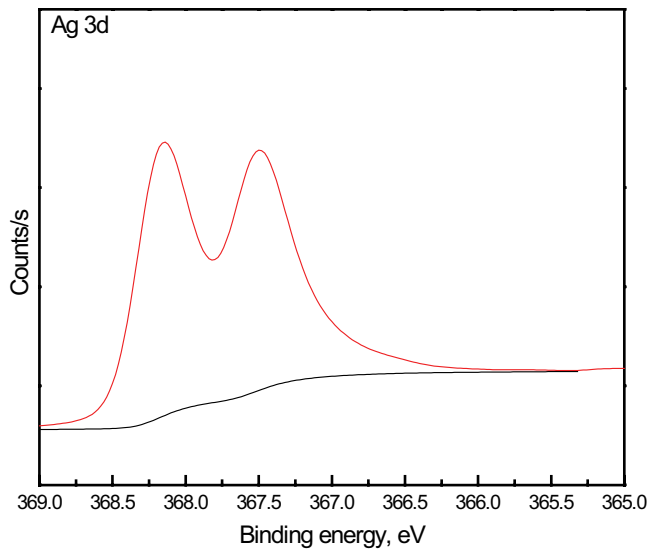


Fig. 4. XPS spectra for Ag3d in the AGZ-1.2 sample.

Table 1  
BET surface area for the Z and AGZ samples

Sample	$S_{\text{BET}}$ (m <sup>2</sup> /g)
Z	60
AGZ-0.4	56
AGZ-0.8	53
AGZ-1.2	50
AGZ-1.6	48

surface area for zinc oxide. These results show that there are two factors affecting the photocatalytic activity of zinc oxide, namely the higher surface area due to the nanowire structure and the decrease in the bandgap by the doping of silver onto the zinc oxide surface as discussed in the next paragraph. Additionally, the addition of silver on the zinc oxide surface decreases BET by blocking some of the pores in the zinc oxide.

Fig. 5 shows the UV-Vis spectra for the Z, AGZ-0.4, AGZ-0.8, AGZ-1.2, and AGZ-1.6 samples. These data show that the ZnO absorbs in the UV region and that the addition of silver to the zinc oxide nanowires leads to a shift in the absorption band for the zinc oxide from the UV region to the visible region. The values for the bandgap energies were calculated using the UV-Vis spectra measured for the Z, AGZ-0.4, AGZ-0.8, AGZ-1.2, and AGZ-1.6 samples. The bandgaps for the Z, AGZ-0.4, AGZ-0.8, AGZ-1.2, and AGZ-1.6 samples are 3.20, 2.80, 2.70, 2.62, and 2.61 eV, respectively as shown in Table 2.

Fig. 6 shows PL spectra for the Z, AGZ-0.4, AGZ-0.8, AGZ-1.2, and AGZ-1.6 samples. The Z sample shows a high PL peak intensity, with the addition of silver to the ZnO nanowires decreasing the position and intensity of the PL peak. The values for the bandgap energies for the Z, AGZ-0.4, AGZ-0.8, AGZ-1.2, and AGZ-1.6 samples calculated from their PL emission spectra are 3.21, 2.81, 2.71, 2.63, and 2.62,

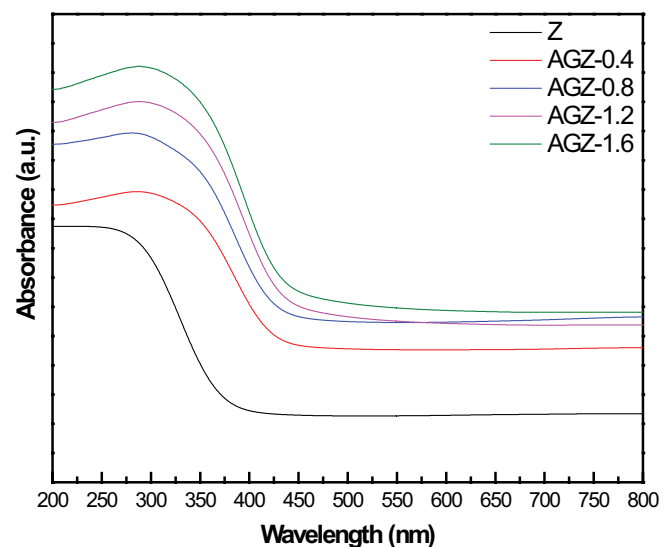


Fig. 5. UV-Vis spectra for the Z, AGZ-0.4, AGZ-0.8, AGZ-1.2, and AGZ-1.6 samples.

Table 2  
Bandgap energy for the Z and AGZ samples

Sample	$S_{\text{BET}}$ (m <sup>2</sup> /g)
Z	3.2
AGZ-0.4	2.80
AGZ-0.8	2.70
AGZ-1.2	2.62
AGZ-1.6	2.61

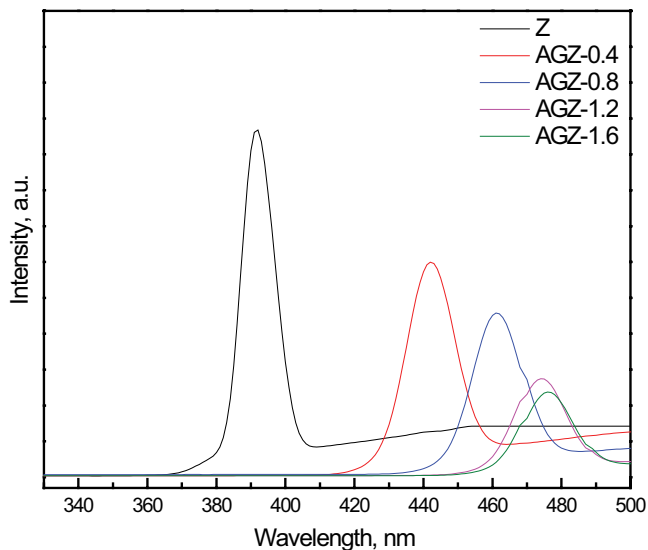


Fig. 6. PL spectra for the Z, AGZ-0.4, AGZ-0.8, AGZ-1.2, and AGZ-1.6 samples.

respectively. These values are very close to those obtained from the UV-Vis spectra as discussed in the previous paragraph.

### 3.2. Photocatalytic performance

As mentioned earlier, the reduction of the mercury ion was utilized to test the synthesized photocatalyst. Fig. 7 shows the effect of the silver weight percent on the mercury ion reduction. The photocatalytic reduction of the mercury ion with use of the Z sample is very small (4%); this can be explained by the fact that the Z sample absorbs only in the UV region while the light source used covers the visible region. The photocatalytic reduction of the mercury ion with use of the AGZ-0.4, AGZ-0.8, AGZ-1.2, and AGZ-1.6 samples were at 50%, 85%, 99%, and 100%, respectively. It is clear that the addition of silver increases the photocatalytic reduction of the mercury ion. The AGZ-1.2 sample exhibits superior efficiency with an approximately 99% conversion.

The effect of the amount of catalyst added to the reaction was also studied. Fig. 8 shows the effect of the dose of the AGZ-1.2 photocatalyst on the photocatalytic reduction of the mercury ion. By increasing the dose from 0.3 to 0.6 g/L, the photocatalytic reduction of the mercury ion increased from 65% to 99%, respectively. By increasing the dose of the AGZ-1.2 photocatalyst from 0.6 to 1.2 g/L, the reaction time

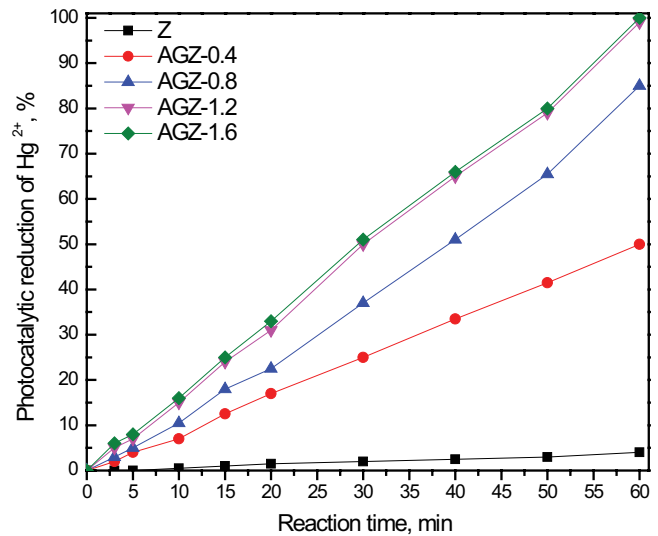


Fig. 7. Effect of varying the weight percent of silver on photocatalytic reduction of the mercury ion.

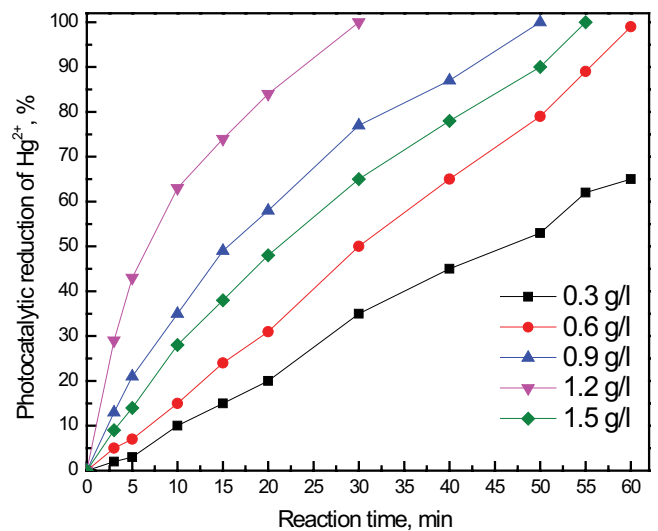


Fig. 8. Effect of the dose of the AGZ-1.2 photocatalyst for photocatalytic reduction of the mercury ion.

required for a complete photocatalytic reduction of the mercury ion decreased from 60 to 30 min, respectively. This may be due to an increased number of available active sites due to the increased photocatalyst dose. If the dose was raised above 1.2 g/L to a value of 1.5 g/L, the reaction time required for complete photocatalytic reduction of the mercury ion increased from 30 to 55 min. Increasing the dose of the photocatalyst beyond a certain point may hinder the penetration of light to reach all the active sites on the photocatalyst.

A test for the possibility of the reuse of the catalyst was also performed. Fig. 9 shows recycling and reuse of the AGZ-1.2 photocatalyst for the photocatalytic reduction of the mercury ion. This figure shows that the photocatalytic reduction of the mercury ion remains constant even if the catalyst is reused five times, indicating great stability for the AGZ-1.2 photocatalyst.

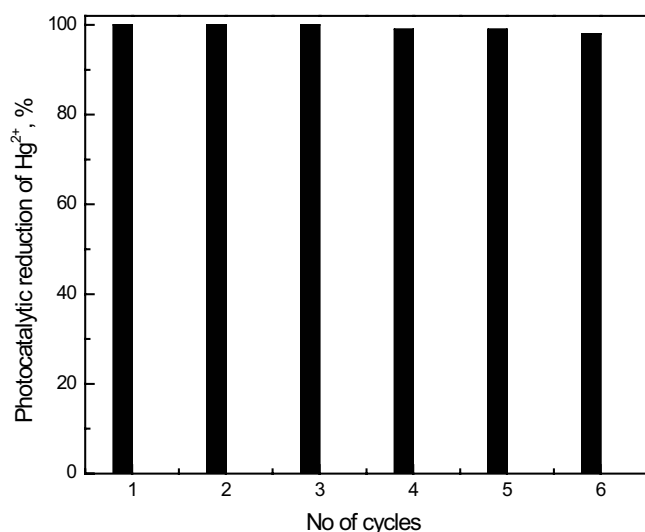


Fig. 9. Recycling and reuse of the AGZ-1.2 photocatalyst for photocatalytic reduction of the mercury ion.

#### 4. Conclusions

Uniform Z and AGZ nanowire samples were produced by a sol-gel method. The reduction of mercury ions was utilized to test the synthesized photocatalysts under visible light. The values for the specific surface area of the Z, AGZ-0.4, AGZ-0.8, AGZ-1.2, and AGZ-1.6 samples were determined to be 60, 56, 53, 50, and 48 m<sup>2</sup>/g, respectively, which indicate that the Z sample shows a higher BET surface area compared with the AGZ samples. The Z and AGZ samples show a nanowire shape, as determined by TEM. The photocatalytic performance for the nanocomposites was studied by mercury(II) reduction under visible light. In terms of photocatalytic performance for mercury(II) reduction, AGZ-1.2 outperforms AGZ-1.6 by 0.99 times, AGZ-0.8 by 1.2 times, AGZ-0.4 by 1.98 times, and Z by 24.75 times.

#### Acknowledgment

The authors would like to express their gratitude to King Khalid University, Saudi Arabia, for providing administrative and technical support.

#### References

- [1] W.J. Patterson, Wastewater Treatment Technology, Ann Arbor Science, Michigan, 1975.
- [2] R.D. Cassidy, A. Furr, Toxicity of Heavy Metals in the Environment, Part 1, F.W. Oehme, Ed., Marcel Dekker, New York, 1978.
- [3] U.S.E.P.A., Mercury Study Report to Congress, EPA-425/R-97-006, Office of Air Quality Planning & Standards and Office of Research and Development, 1997.
- [4] F. Zahir, S.J. Rizwi, S.K. Haq, R.H. Khan, Low dose mercury toxicity and human health, Environ. Toxicol. Pharmacol., 20 (2005) 351–360.
- [5] U.N.E.P. Chemicals, Global Mercury Assessment, Report no. 54790-01, Geneva, 2002.
- [6] J.M. Hammer, Water and Waste-Water Technology, Wiley, New York, 1975.
- [7] A. Pamalho, Introduction to Wastewater Treatment Processes, Academic Press, London, 1977.
- [8] N. Serpone, K. Ah-You, T.P. Tran, R. Harris, AM1 simulated sunlight photoreduction and elimination of Hg(II) and CH<sub>3</sub>Hg(II) chloride salts from aqueous suspensions of titanium dioxide, Sol. Energy, 39 (1987) 491–498.
- [9] M.A. Aguado, S. Cervera-March, J. Gimenez, Continuous photocatalytic treatment of mercury(II) on titania powders: kinetics and catalyst activity, Chem. Eng. Sci., 50 (1995) 1561–1569.
- [10] S.G. Botta, D.J. Rodriguez, A.G. Leyva, M.I. Litter, Features of the transformation of Hg-II by heterogeneous photocatalysis over TiO<sub>2</sub>, Catal. Today, 76 (2002) 247–258.
- [11] L.B. Khalil, M.W. Rophael, W.E. Mourad, The removal of the toxic Hg(II) salts from water by photocatalysis, Appl. Catal., B, 36 (2002) 125–130.
- [12] X. Wang, S.O. Pehkonen, A.K. Ray, Photocatalytic reduction of Hg(II) on two commercial TiO<sub>2</sub> catalysts, Electrochim. Acta, 49 (2004) 1435–1444.
- [13] U.S.E.P.A., Water Quality Criterion for the Protection of Human Health: Methyl Mercury, EPA-823-R-01-001, Office of Science and Technology and Office of Water, 2001.
- [14] J. Aguado, R. van Grieken, M. Lopex-Munoz, J. Marugan, A comprehensive study of the synthesis, characterization and activity of TiO<sub>2</sub> and mixed TiO<sub>2</sub>/SiO<sub>2</sub> photocatalysts, Appl. Catal., A, 312 (2006) 202–212.
- [15] C. Anderson, A.J. Bard, Improved photocatalytic activity and characterization of mixed TiO<sub>2</sub>/SiO<sub>2</sub> and TiO<sub>2</sub>/Al<sub>2</sub>O<sub>3</sub> materials, J. Phys. Chem. B, 101 (1997) 2611–2616.
- [16] K.Y. Jung, S.B. Park, Enhanced photoactivity of silica-embedded titania particles prepared by sol-gel process for the decomposition of trichloroethylene, Appl. Catal., B, 25 (2000) 249–256.
- [17] P. Pucher, M. Benmami, R. Azouani, G. Krammer, K. Chhor, J.F. Bocquet, A.V. Kanaev, Nano-TiO<sub>2</sub> sols immobilized on porous silica as new efficient photocatalyst, Appl. Catal., A, 332 (2007) 297–303.
- [18] E. Pitoniak, C.Y. Wu, D. Londeree, D. Mazyck, J.C. Bonzongo, K. Powers, W. Sigmund, Nanostructured silica-gel doped with TiO<sub>2</sub> for mercury vapor control, J. Nanopart. Res., 5 (2003) 281–292.
- [19] H.E. Byrne, W.L. Kostedt, J.M. Stokke, D.W. Mazyck, Characterization of HF catalyzed silica gels doped with Degussa P<sub>25</sub> titanium dioxide, J. Non-Cryst. Solids, 355 (2009) 525–530.
- [20] E. Pitoniak, C.Y. Wu, D.Q. Mazyck, K.W. Powers, W. Sigmund, Adsorption enhancement mechanisms of silica-titania nanocomposites for elemental mercury vapor removal, Environ. Sci. Technol., 39 (2005) 1269–1274.
- [21] J.M. Stokke, D.W. Mazyck, Development of a regenerable system employing silica-titania composites for the recovery of mercury from end-box exhaust at a chlor-alkali facility, J. Air Waste Manage. Assoc., 58 (2008) 530–537.
- [22] J.M. Stokke, D.W. Mazyck, C.Y. Wu, R. Sheahan, Photocatalytic oxidation of methanol using silica-titania composites in a packed-bed reactor, Environ. Prog., 25 (2006) 312–318.
- [23] J.L. Parker, N.S. Bloom, Preservation and storage techniques for low-level aqueous mercury speciation, Sci. Total Environ., 337 (2005) 253–263.
- [24] A. Kanta, R. Sedev, J. Ralston, Thermally and photoinduced changes in the water wettability of low-surface-area silica and titania, Langmuir, 21 (2005) 2400–2407.
- [25] A. Kanta, R. Sedev, J. Ralston, Preparation of silica-on-titania patterns with a wettability contrast, Langmuir, 21 (2005) 5790–5794.
- [26] H. Zhang, Photochemical redox reactions of mercury, Struct. Bond., 120 (2006) 37–79.
- [27] C. Tian, Q. Zhang, A. Wu, M. Jiang, Z. Liang, B. Jiang, H. Fu, Cost-effective large-scale synthesis of ZnO photocatalyst with excellent performance for dye photodegradation, Chem. Commun., 48 (2012) 2858–2860.
- [28] B. Li, T. Liu, Y. Wang, Z. Wang, ZnO/graphene-oxide nanocomposite with remarkably enhanced visible-light-driven photocatalytic performance, J. Colloid Interface Sci., 377 (2012) 114–121.
- [29] A.Y.S. Malkhasian, R.M. Mohamed, Environmental remediation of Cr(VI) solutions by photocatalytic reduction using Ag-Er(OH)<sub>3</sub> nanocomposite, J. Alloys Compd., 632 (2015) 735–740.